Supplementary Information

Bimetallic Tungstate Nanoparticle-decorated-lignin Electrodes for Flexible Supercapacitors†

Swarn Jha,[a] Siddhi Mehta,[b] Eugene Chen,[b] Selvasundarasekar Sam Sankar,[c] Subrata Kundu,[c,*] and Hong Liang,[a,b,*]

[a] J. Mike Walker '66 Department of Mechanical Engineering, Texas A&M University, 202 Spence Street, College Station, TX 77843-3123, USA E-mail: swarn.jha14@tamu.edu
[b] Department of Materials Science & Engineering, Texas A&M University, 202 Spence Street, College Station, USA E-mail: siddhi_23@tamu.edu
[c] Materials Electrochemistry (ME) Division, CSIR-Central Electrochemical Research Institute (CECRI), Karaikudi, Tamilnadu-630003, India. E-mail: skundu@cecri.res.in
[*] Corresponding author: hliang@tamu.edu, Telephone: (979) 862-2623, Fax no.: 979-845-3081
[†] Electronic supplementary information (ESI) available: Synthesis of nanoparticles; XPS spectra of $CoWO_4$ nanoparticles; optical microscope images of electrodes; Interferometer images of electrodes; table summary for electrochemical experiments; table for performance comparison with literature reports.

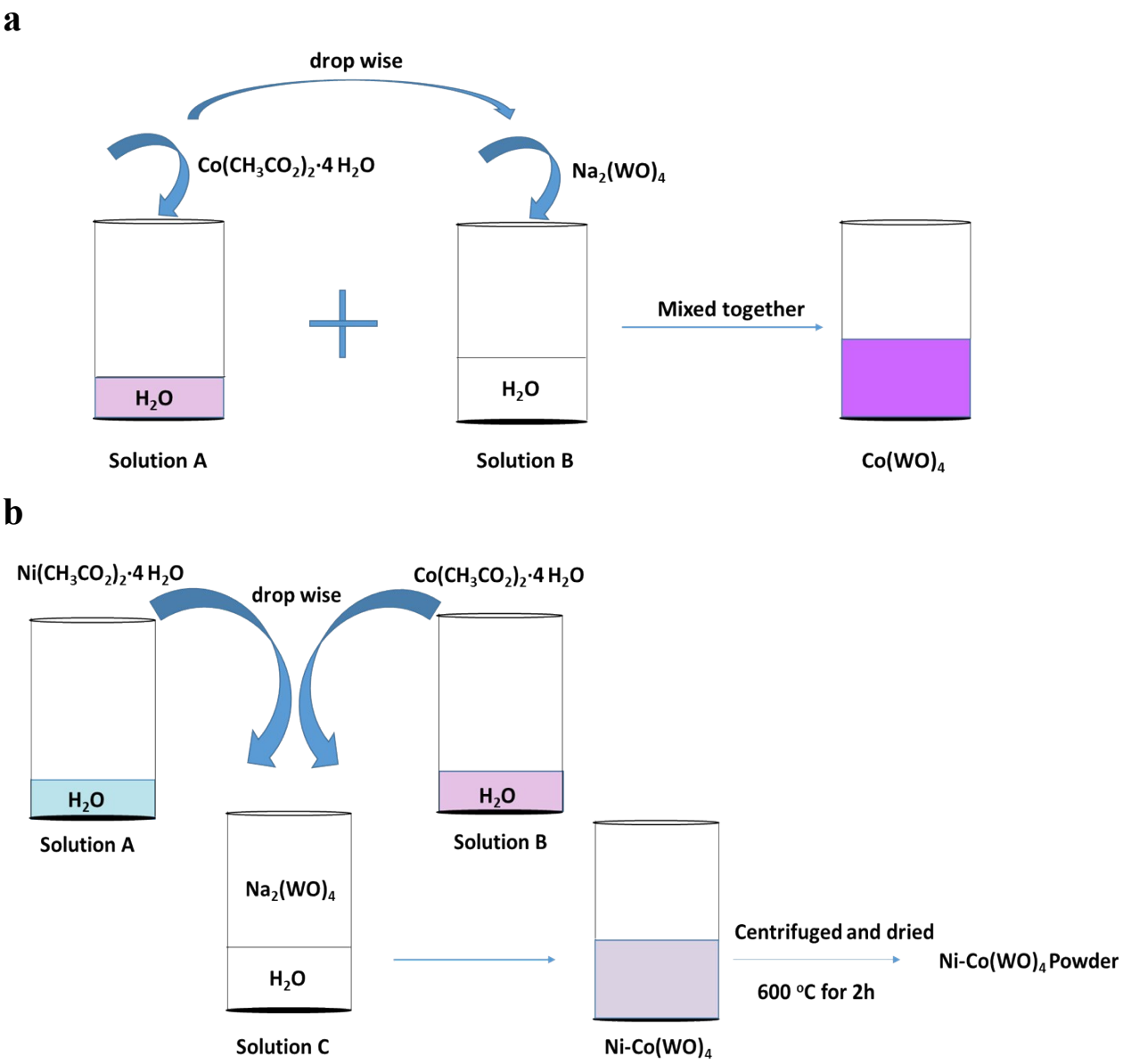

Fig. S1. Synthesis of (a) $CoWO_4$, and (b) Ni-$CoWO_4$ nanoparticles.

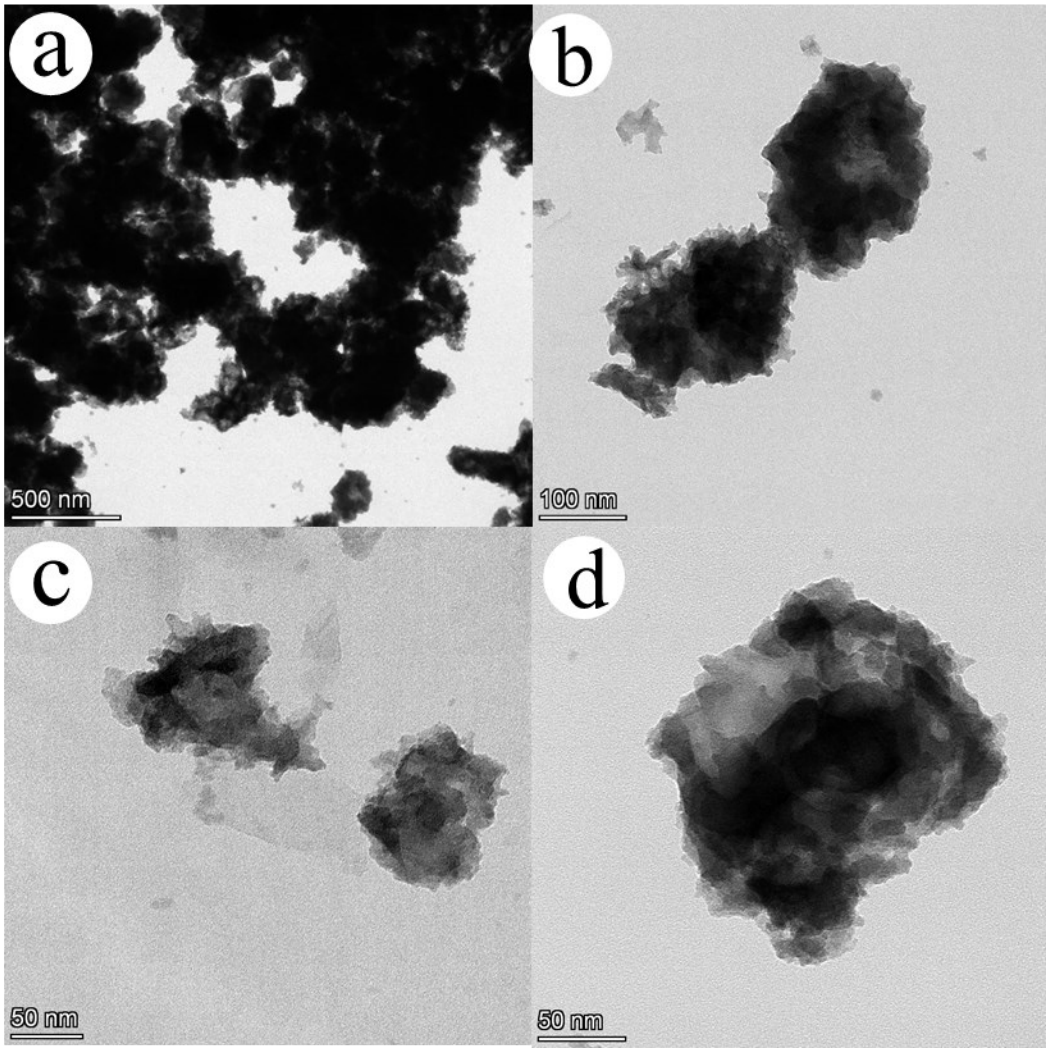

Fig. S2. (a-d) are the low and high magnified HR-TEM microscopic images of Ni-$CoWO_4$.

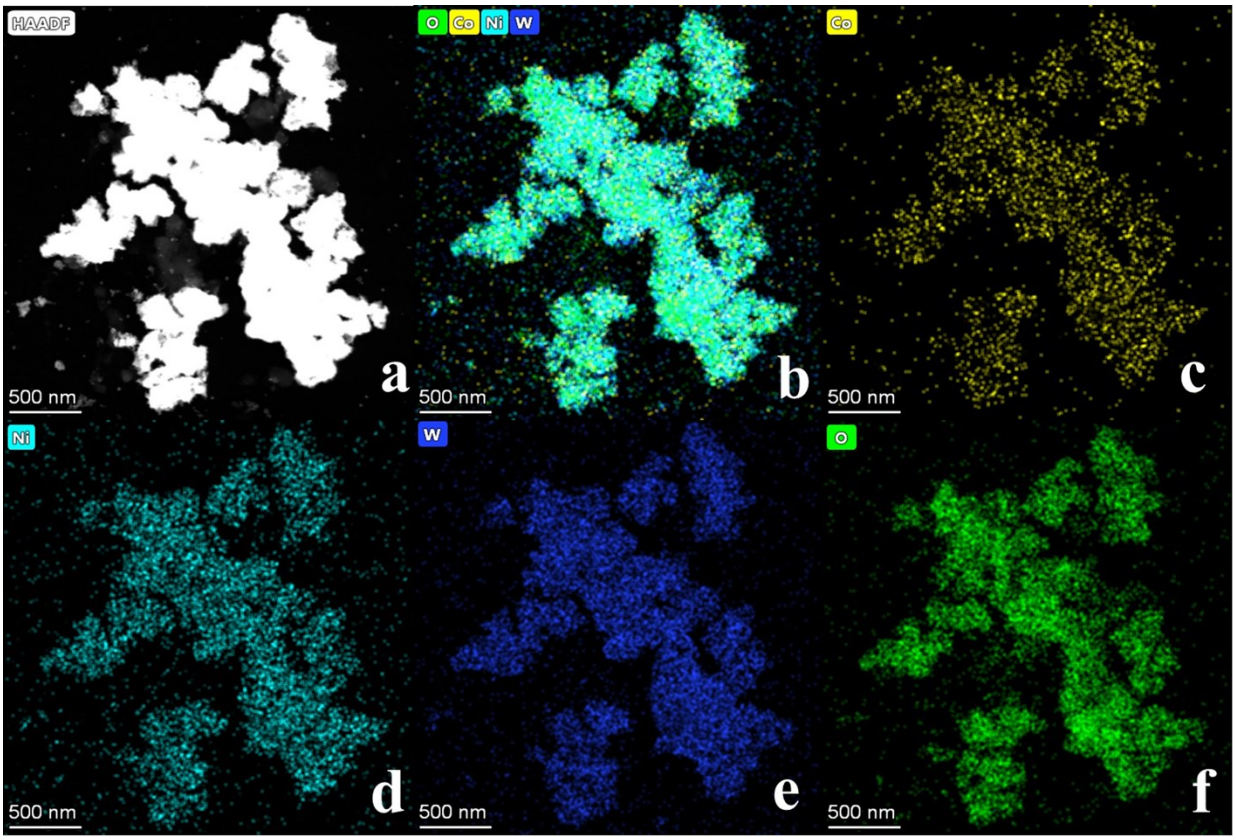

Fig. S3(a-f). 'a' is a HAADF image of Ni-$CoWO_4$, 'b' is the image of mixed elemental distribution, (c-f) are corresponds to mapping results of Cobalt, Nickel, Tungsten and Oxygen respectively.

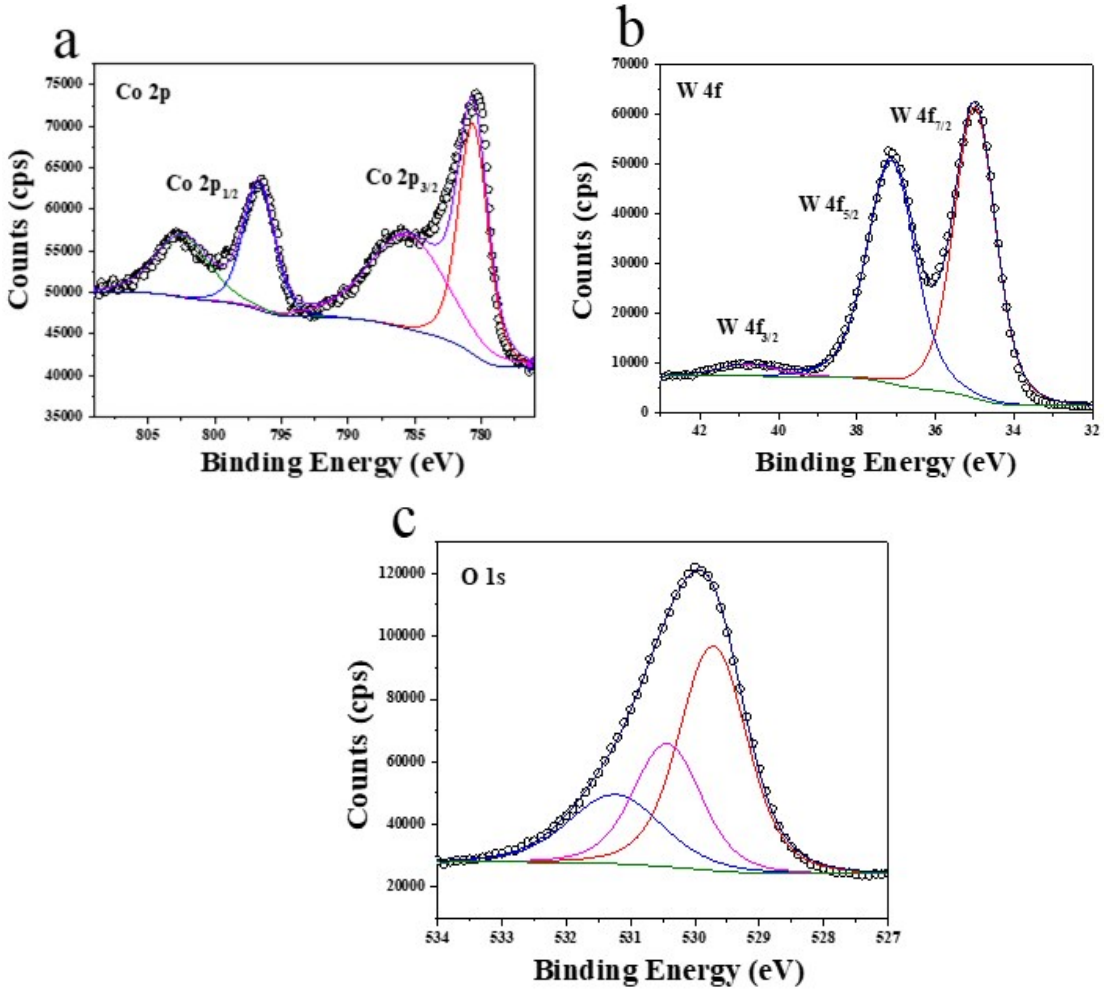

Fig. S4. XPS Spectrum for: (a) Co 2p, (b) W 4f, and (c) O 1s.

For identifying the nature of the elements, X-ray photoelectron spectroscopy (XPS) was carried out. The subsequent high-resolution XPS spectrum is shown in Fig. S4(a-c) and 5(a-d). Fig. S4a is the high-resolution XPS spectrum of Co 2p. The binding energy values of 796.72 and 780.75 eV correspond to Co 2p 1/2 and Co 2p 3/2 and the corresponding satellite peaks were observed at 785.72 and 802.52 eV respectively. This shows cobalt is present in a +2 oxidation state. The high-

resolution spectrum is shown in Fig. S4b corresponds to W 4f. Herein, the binding energy values of 40.78, 35.0, and 37.11 eV correspond to W 4f 3/2, W 5p 7/2, and W 4f 5/2, respectively. Fig. S2c is the high-resolution XPS spectrum of O 1s where the observed binding energies are 529.7, 530.4, and 531.2 eV corresponding to metal oxide and lattice oxygen of $CoWO_4$.

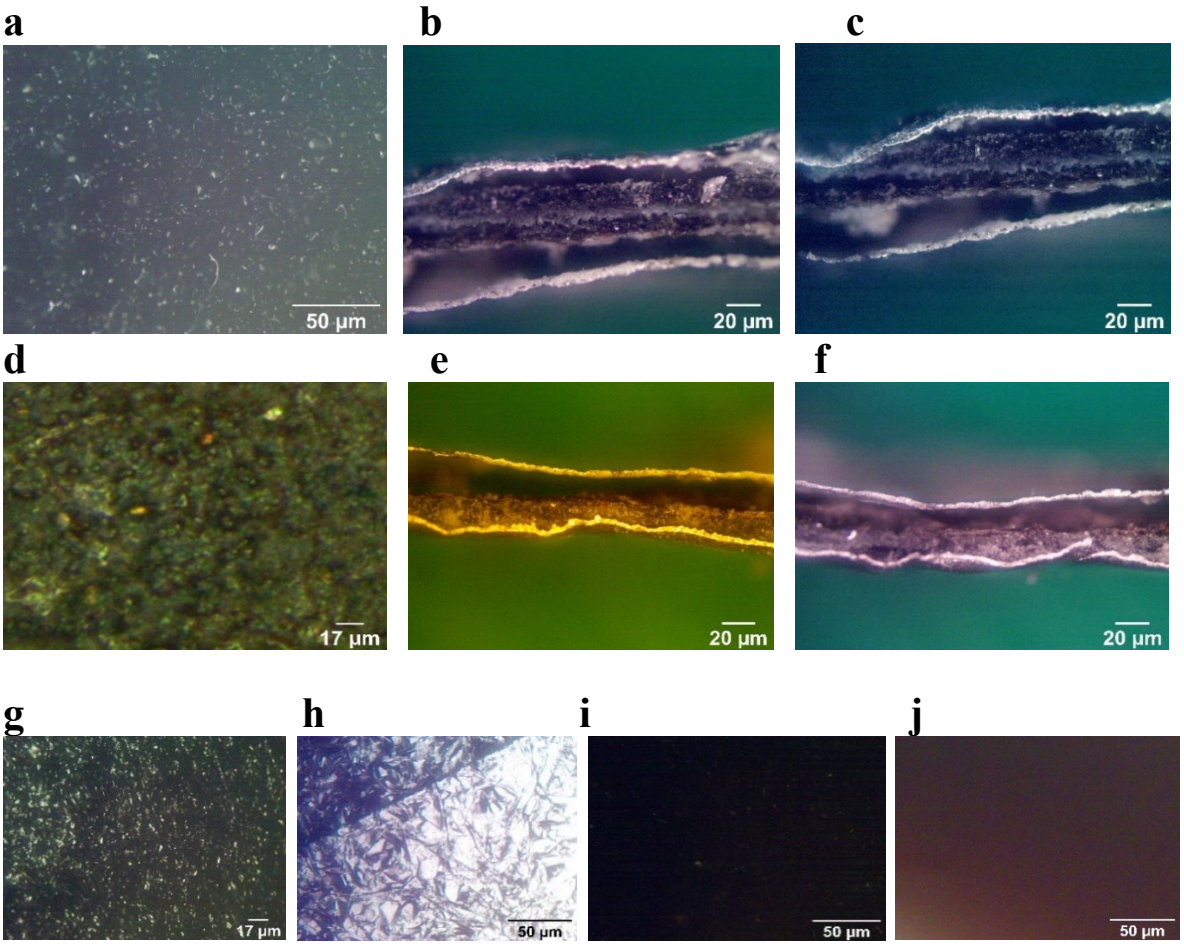

Fig. S5. OM images for (a) lig-$CoWO_4$ electrode surface, composite lignin/$CoWO_4$ supercapacitor interface before testing (b) and after testing (c), electrode surface of lig-Ni-$CoWO_4$ (d), composite lignin/Ni-$CoWO_4$ electrode before testing (e) and after testing (f); and electrode surfaces of graphene electrode at low magnification (g) and high magnification (h), activated carbon electrode (i), and alkali lignin electrode (j).

3.5 Micrographs and configuration of the supercapacitor electrodes and interface

Optical microscopy (OM) was performed to observe the surface features of the electrodes and the interface of the supercapacitor (Fig.S5(a-j)). Fig. S5a and Fig. S5d show the $CoWO_4$ nanoparticle-infused lignin electrode and the $NiCoWO_4$ infused lignin electrode surfaces respectively. $CoWO_4$ NP (white) appear embedded (Fig. S5a) and uniformly distributed across the lignin matrix (dark). Similarly, the $NiCoWO_4$ particles (yellowish) appear homogeneously spread across the lignin matrix (dark greenish). In both Fig. S5a and Fig. S5d, there is no evidence of any surface aberration, damage, or mechanical deformation which are essential for the mechanical integrity of the electrodes. Also, the even distribution of NP in the lignin matrix is critical for the homogeneity of surface reactions. Comparing the lignin-$CoWO_4$ supercapacitor's interface before (Fig. S5b) and after (Fig. S5c) electrochemical testing, it is ascertained that the interface is intact and does not change as much. Similarly, the lignin-NiCoWO4 supercapacitor's interface before (Fig. S5e) and after (Fig. S5f) electrochemical testing shows evidence of intactness. This is important for stable performance during cycling. The interface thickness is about 40 μm. The thin layer graphene electrode surface is shown both in low (200x) magnification (Fig. S5g) and a high (400x) magnification, (Fig. S5h). The graphene electrode appears shinier than the AC electrode surface (Fig. S5i). This is due to a comparatively higher light reflectance from the thin graphene layer [1-4]. Also, the higher magnification image (Fig. S5h) shows uniform wrinkles like surface morphology whereas those of AC (Fig. S5i) and lignin electrode surface (S5j) show a higher degree of light absorption on account of more surface defects and complex 3D network of chains.

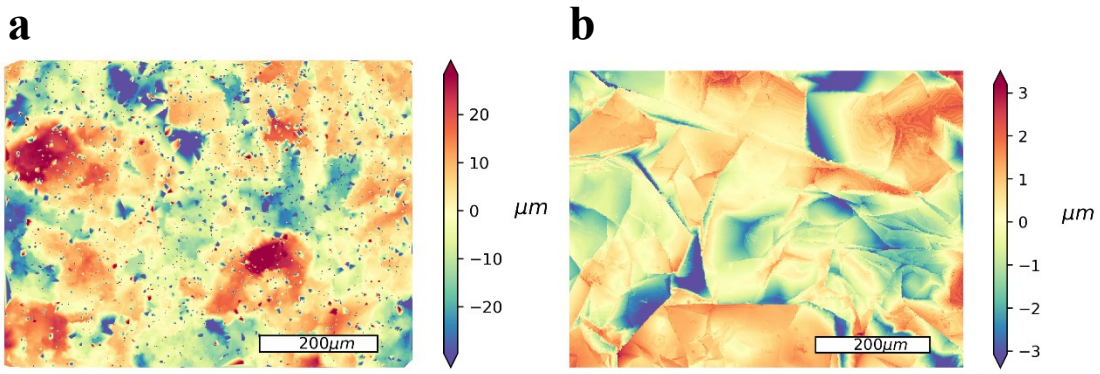

Fig. S6. Interferometer images for: (a) AC electrode and (b) graphene electrode. Surface roughness is depicted by the color scale bars (μm) to the right of each figure.

3.6 Topography of the supercapacitor electrodes

The negative electrode's surface roughness plays a vital role in influencing a supercapacitor's electrochemical performance. A rougher surface leads to more contact with the electrolyte, thus, leading to an enhanced area for charge transport. However, surface roughness also hampers the mechanical integrity of the interface. So, the challenge is obtaining an electrode surface which has just about enough surface roughness that it does not create problems of interface instability during device operation. The carefully prepared cathodes of AC (Fig. S6a) and graphene (Fig. S6b) were studied for surface roughness profiles using an interferometer. The AC electrode surface roughness ranges from 0 - 20 μm whereas, for the graphene electrode, it ranges from 0-3 μm suggesting a higher average roughness for the AC electrode. For the AC electrode, surface roughness is more or less uniformly distributed with some patches of higher roughness (red patches in Fig. S6a). For the graphene electrode, there can be seen localized patches of red and blue. The patches diffuse out to different color zones more smoothly.

Table S1. Summary of Electrochemical Experiments.

Test Name	Specific Capacitance (mF cm^{-2})	Retention (%)	
Effect of Ni			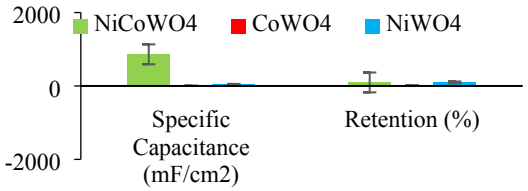
$NiCoWO_4$	862.26	96.12	
$CoWO_4$	6.10	14.90	
$NiWO_4$	32.90	98.20	
Effect of mass loadings - lignin/$NiCoWO_4$			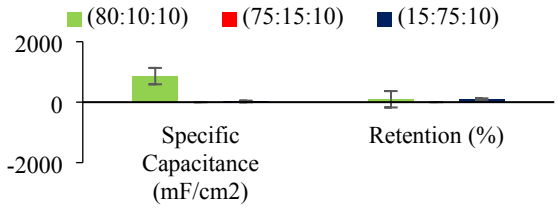
(80:10:10)	862.26	96.12	
(75:15:10)	1.14	51.91	
(15:75:10)	23.88	100	
Effect of discharge time - lignin/$NiCoWO_4$ (75:15:10)			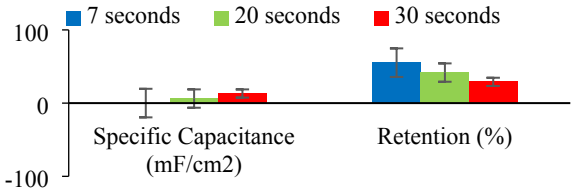
7 seconds	0.06	55.25	
20 seconds	6.24	41.72	
30 seconds	13.13	29.03	
Effect of Carbonization - (75:15:10)			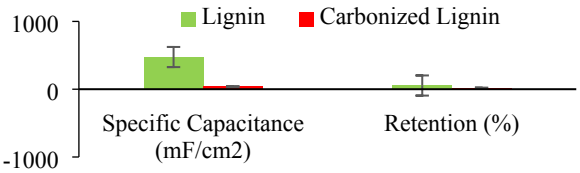
Lignin	474.68	54.47	
Carbonized Lignin	38.10	15.19	
Effect of the negative electrode (75:15:10)			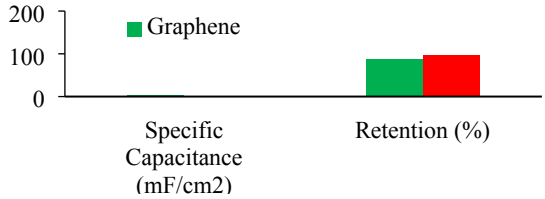
Graphene	4.03	88.59	
AC	1.14	97.56	
Effect of the negative electrode (15:75:10)			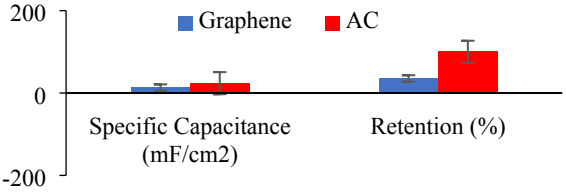
Graphene	13.13	35.27	
AC	23.88	99.97	

Table S2. Comparison of the electrochemical performance of the designed supercapacitor using lig-NiCoWO4 materials with literature reports.

Electrode Active Materials/Substrate	Specific Capacitance (mF cm^{-2})	Current Density (mA cm^{-2})	Energy Density	Power Density	This work/ Lit report	Ref.
Al//lignin-Ni-$CoWO_4$	862.26 (2000 cycles)	800	5.75 Wh kg^{-1}	854.75 kW kg^{-1}	-	This work
Ni Foam//$ZnCo_2O_4$	94 (1400 cycles)	0.1	-	-	9.17	[5]
Ni Foam//$NiCo_2O_4$	161 (3000 cycles)	3	-	-	5.35	[6]
PET/PDMS//Graphene fibers/MnO_2 fibers	42.02 (1000 cycles)	1	1.46×10^{-3} mWh cm^{-2}	0.69 mW cm^{-2}	20.52	[7]
PET//Au-polyaniline	51.7 (1000 cycles)	0.1	5.57 mWh cm^{-3}	0.33 W cm^{-3}	16.68	[8]
PET//Ag-AC	45 (1200 cycles)	0.3	-	-	19.16	[9]
Au wire//MnO_2	12 (2000 cycles)	0.3	5.4 $\mu W \cdot h \cdot cm^{-2}$	-	71.86	[10]
Al//AC/Lignin-MnO_2	5.52 (2000 cycles)	0.13	14.1 Wh kg^{-1}	1000 W kg^{-1}	156.21	[11]
CW-PNC-PEDOT//CW-CMK-3	31.6 (2000 cycles)	0.4 (1400 cycles)	0.011 mWh cm^{-2}	7.8 mW cm^{-2}	27.28	[12]
Al//lignin-$NiWO_4$	17.01 (2000 cycles)	0.13 (2000 cycles)	2	100	50.69	[13]
$CoCO_3$//AC	215 (1000 cycles)	1.5 (1000 cycles)	-	-	4.02	[14]

References

1. A. Dillner and S. J. A. M. T. Takahama, 2015, **8**.
2. S. Duber, J. N. Rouzaud, C. Clinard and S. Pusz, *Fuel Processing Technology*, 2002, **77-78**, 221-227.
3. N. Jung, B. Kim, A. C. Crowther, N. Kim, C. Nuckolls and L. J. A. N. Brus, 2011, **5**, 5708-5716.
4. H. S. Skulason, P. E. Gaskell and T. Szkopek, *Nanotechnology*, 2010, **21**, 295709.
5. R. K. Gupta, J. Candler, S. Palchoudhury, K. Ramasamy and B. K. Gupta, *Scientific Reports*, 2015, **5**, 15265.
6. Q. Wang, X. Wang, B. Liu, G. Yu, X. Hou, D. Chen and G. Shen, *Journal of Materials Chemistry A*, 2013, **1**, 2468-2473.
7. X. Li, T. Zhao, Q. Chen, P. Li, K. Wang, M. Zhong, J. Wei, D. Wu, B. Wei and H. Zhu, *Physical Chemistry Chemical Physics*, 2013, **15**, 17752-17757.
8. K. Zhang, H. Hu, W. Yao and C. Ye, *Journal of Materials Chemistry A*, 2015, **3**, 617-623.
9. H. Lee, S. Hong, J. Kwon, Y. D. Suh, J. Lee, H. Moon, J. Yeo and S. H. Ko, *Journal of Materials Chemistry A*, 2015, **3**, 8339-8345.
10. H. Xu, X. Hu, Y. Sun, H. Yang, X. Liu and Y. Huang, *Nano Research*, 2015, **8**, 1148-1158.
11. S. Jha, S. Mehta, Y. Chen, L. Ma, P. Renner, D. Y. Parkinson and H. Liang, *ACS Sustainable Chemistry & Engineering*, 2020, **8**, 498-511.
12. M. Zheng, L. Li, P. Gu, Z. Lin, W. Du, H. Xue and H. Pang, 2017, **5**, 544-548.
13. S. Jha, S. Mehta, Y. Chen, P. Renner, S. S. Sankar, D. Parkinson, S. Kundu and H. Liang, *Journal of Materials Chemistry C*, 2020, DOI: 10.1039/C9TC05811G.
14. H. Yang, H. Xu, M. Li, L. Zhang, Y. Huang and X. Hu, *ACS Applied Materials & Interfaces*, 2016, **8**, 1774-1779.